UNIVERSITÀ DI PARMA

ARCHIVIO DELLA RICERCA

University of Parma Research Repository

Impact of the Interplay Between Mode Dispersion and Kerr Effect in SDM Optical Networks

This is the peer reviewd version of the followng article:

Original
Impact of the Interplay Between Mode Dispersion and Kerr Effect in SDM Optical Networks / Sambo, N., Lasagni, C., Serena, P., Castoldi, P., Bononi, A.. - In: JOURNAL OF LIGHTWAVE TECHNOLOGY. - ISSN 0733-8724. - 41:6(2023), pp. 1603-1609. [10.1109/JLT.2022.3228595]

Availability:
This version is available at: 11381/2950072 since: 2023-06-30T13:53:21Z

Publisher:
Institute of Electrical and Electronics Engineers Inc.

Published
DOI:10.1109/JLT.2022.3228595

Terms of use:

Anyone can freely access the full text of works made available as "Open Access". Works made available

Publisher copyright

note finali coverpage

(Article begins on next page)

15 October 2026

Impact of the interplay between mode dispersion and Kerr effect in SDM optical networks

Nicola Sambo, Chiara Lasagni, *Member, IEEE,* Paolo Serena, *Senior Member, IEEE,* Piero Castoldi, *Senior Member, IEEE,* and Alberto Bononi *Senior Member, IEEE*

***Abstract*—Space division multiplexing (SDM) – such as based on multi-mode fibers – is under investigation to support the growing capacity demands. In optical networks, the estimation of quality of transmission (QoT) is a fundamental control task to identify the most suitable transmission parameters (e.g., modulation format) to meet proper spectral efficiency while satisfying the required optical reach. The Gaussian Noise (GN) model is widely adopted for QoT estimation. However, the basic version of the GN model does not account for the interplay between mode dispersion and the Kerr effect.**

In this paper, we investigate the impact of mode dispersion on SDM networks exploiting strongly coupled modes, through an extended GN model. Network performance analysis is evaluated. First, an analysis of the achievable information rate (AIR) with Gaussian data statistics is presented. Then, a network capacity analysis is shown constrained to a set of supported modulation formats and a fixed symbol rate. Finally, blocking probability is studied with the same set of supported modulation formats with variable symbol rates. The presented network analysis shows that accounting for mode dispersion increases the throughput considering: i) Gaussian data statistics, ii) different modulation formats. Moreover, the blocking probability analysis shows a blocking reduction when mode dispersion is considered in the physical layer modeling.

***Index Terms*—SDM, multi-mode fibers, multi-core fibers, mode dispersion, GN model, Gaussian noise model**

I. Introduction

NETWORKS based on space-division multiplexing (SDM) with parallel fibers, multi-core (MCFs), or multi-mode fibers (MMFs) are under investigation to support the growing capacity demand [1]. Assuming the availability of amplifiers to handle multiple modes/cores, MCFs or MMFs – with respect to parallel fibers – permit to adopt a single amplifier for all the available space dimensions over the same fiber [2]–[5]. Several limitations have already been resolved, such as linear inter-modal crosstalk and the different delays among the modes and the polarizations, i.e., mode dispersion (MD), that are efficiently equalized by multiple-input multiple-output (MIMO) coherent receivers [6], [7]. The complexity of the MIMO does not seem to be a limiting factor, even in submarine applications [8]. As a matter of fact, commercial add&drop multiplexers are already available handling 15 modes with multiplane light conversion technology [9], [10].

Several investigations then focused on transmission modelling. Quality of transmission (QoT) studies have been performed extending the widely adopted Gaussian Noise (GN) model [11], [12] to account for the novel modal (spatial) dimension [13] and for inter-modal crosstalk [14], [15]. The GN model is conservative, aiming at assuring that established channels do not experience worse physical layer performance than the estimated ones, thus avoiding possible outages. Conservative assumptions are typically adopted by network operators, as an example through network margins to account for time-variant or traffic dependent effects [16], [17], such as aging or environmental effects. Network margins aim at assuring that established channels do not experience outages during their life, even if physical conditions get worse.

Despite its wide use, the basic GN model does not account for the interplay between MD and the Kerr nonlinearity among the propagating optical modes. Such an interplay has been shown in the limit of high MD [18] to be beneficial in strongly coupled fibers to mitigate the nonlinear effect, provided that linear MD is fully compensated at the receiver. An extension of the GN model to include arbitrary values of MD in strongly coupled SDM fibers has been recently shown and validated in [19], with both a semi-analytical and a simplified formula. The corresponding model has been called the ergodic GN model. Since MD in fibers supporting SDM is much higher than the polarization mode dispersion (PMD) experienced by single-mode fibers (SMF), by factors up to hundred of thousand times higher [8], its implications on networking are an open research problem.

SDM then has been studied considering networking aspects and significant effort was spent on routing, spectrum, and space-dimension assignment strategies [20]–[27]. Such strategies typically rely on a QoT estimation which accounts for the crosstalk among cores or (groups of) modes. Nevertheless, these studies overlooked the networking implications (e.g., on network capacity) derived from the mitigation of nonlinear effects due to MD.

In this paper, which is an extended version of [28], we exploit the MD-aware ergodic GN model [19] to investigate the gain brought by MD in improving the performance of an SDM network working in a strong coupling regime. Although such a regime implies that the spatial modes are routed together, the MD/Kerr interaction brings some benefits. We will investigate them in network environments from different

This work has been supported by the MIUR PRIN2017 "FIRST" Project (GA 2017HP5KH7_002).

Nicola Sambo and Piero Castoldi are with Scuola Superiore Sant'Anna, Via G. Moruzzi, 1, 56124, Pisa, Italy. nicola.sambo@sssup.it.

Chiara Lasagni is with Università degli Studi dell'Aquila, L'Aquila, Italy.

Paolo Serena and Alberto Bononi are with Università degli Studi di Parma, Parma, Italy.

C. Lasagni, P. Serena, and A. Bononi are also with the CNIT National Laboratory of Advanced Optical Fibers for Photonics (FIBERS), 67100 L.Aquila, Italy.

Manuscript received December 11, 2024.

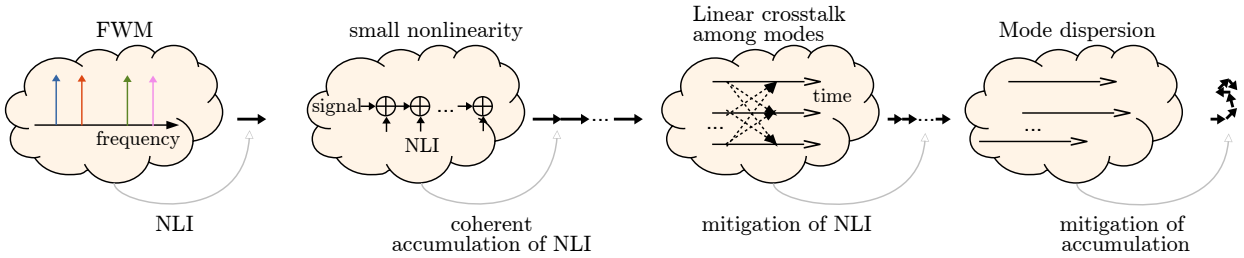

Figure 1: Sketch of transmission impairments. The FWM generates a complex NLI at a given time epoch, here described by the thick arrows, that linearly accumulates during propagation under perturbative assumptions. The linear mode crosstalk mitigates the strength of the accumulation by the Manakov correction factor. The dispersive effects like mode dispersion mitigate the accumulation, through a spatial decorrelation of the NLI during propagation.

perspectives. First, the sub-optimal case of complex Gaussian data statistics will be analyzed when varying the number of modes and the amount of mode dispersion. Then, the network capacity will be analyzed in a network supporting multiple modulation formats at a fixed symbol rate: polarization multiplexing N-ary quadrature amplitude modulation (PM-NQAM), with $N = 8, 16, 32, 64$, and PM-quadrature phase-shift keying (PM-QPSK). Finally, blocking probability will be studied in the presence of multiple modulation formats and symbol rates, also when varying network margins. Differently from [28], a closed-form for the MD-aware GN model is here adopted, and a detailed analysis of the physical layer and of connection blocking probability is provided. The networking analysis carried out will show that the consideration of mode dispersion leads to a more accurate estimation of network capacity, which can be increased.

II. Physical layer modelling

In an SDM network, the information is spread in all the degrees of freedom, i.e., time, frequency, and space. In particular, the propagating spatial modes experience both linear and nonlinear effects within the optical fibers. The general idea is sketched in Fig. 1. The nonlinear Kerr effect induces four-wave mixing (FWM) among the frequencies constituting the propagating signal. As a result of FWM, a nonlinear interference (NLI) appears in each infinitesimal section of the fiber. Under perturbative assumptions, valid with moderate Kerr effect, the received NLI is the sum of all the local NLIs and, in absence of linear effects, would accumulate coherently during propagation. This pessimistic picture is changed by the presence of linear effects. First, SDM transmissions experience linear modal crosstalk which can be induced by design, e.g., by using a multi-core fiber working in the strongly-coupled regime with small inter-core distance, or by random longitudinal imperfections in the fiber. In any case, the presence of linear crosstalk among optical modes induces a quick mixing that can be safely averaged over the typical length scale of the other fiber effects, as per the Manakov equation. As a result, the NLI still accumulates coherently, but with a smaller strength [18]. Such a reduction is more efficient when increasing the number of modes N_m. As a reference, we focus on a strongly coupled multi-core fiber transmission. The NLI variance σ^2_{NLI} without MD on a given channel scales as:

$$\sigma^2_{\mathrm{NLI}}(N_m) \propto (\gamma\kappa)^2(2N_m+1) \propto \frac{1}{2N_m+1} \qquad (1)$$

where we used the scaling for the Kerr coefficient γ equal to $\gamma(N_m) = \gamma_0/N_m$, γ_0 being the nonlinear coefficient of a single core, and the scaling $\kappa(N_m) = \frac{4}{3}\frac{2N_m}{2N_m+1}$ for the Manakov correction factor [18]. The factor $2N_m + 1$ in (1) is related to the scaling of the NLI variance with the number of interfering spatial channels [18], [19]. Overall, (1) suggests a variance reduction inversely proportional to the number of modes.

Second, the presence of dispersive effects, such as MD, induces a channel walk-off that breaks the coherent accumulation during propagation in favor of a partially coherent one. In this way, the total NLI power grows more slowly with distance, see the rightmost graph in Fig. 1, thus making any dispersive effect beneficial, provided that its linear equalization through a MIMO is possible. When the walk-off effect induced by MD is large, the accumulation becomes essentially incoherent, thus yielding the NLI variance to grow linearly with the distance z. The interplay between MD and the Kerr nonlinear effect is quite complex, generating a non-monotone behavior of the general NLI variance with the spatial mode dispersion (SMD) coefficient [19], i.e., a measure of the group delays spread among the strongly coupled modes [8], [19]. While in SMFs such interaction has no practical implications since the SMD coefficient, also known as PMD coefficient, is very small in modern fibers, the case is completely different in fibers supporting SDM where the SMD coefficient usually takes values hundred of times higher [8], [29]. It is worth noting that an SMD coefficient minimizing the cross-phase modulation (XPM) variance exists, of value around 8 ps/$\sqrt{\text{km}}$ [19]. Such a value is thus a benchmark value to investigate the potential of MD in improving the network performance.

Though the interaction between Kerr effect and MD is random because of the random birefringence, making the NLI variance a random variable as well, in [19] it was shown that, at the typical values of SMD, the residual randomness of the NLI variance is of limited importance in strongly coupled SDM networks, such that the average (wrt birefringence) NLI variance is a reliable QoT factor, and a formula to estimate it was proposed. The generalized signal-to-noise ratio (GSNR) – here adopted as figure of merit for QoT – after ideal MIMO

is thus:

$$\text{GSNR} = \frac{P}{\sigma^2_{\text{ASE}} + \mathbb{E}\left[\sigma^2_{\text{NLI}}\right]} \tag{2}$$

with P signal power, σ^2_{ASE} the variance of amplified spontaneous emission noise introduced by the optical amplifiers, σ^2_{NLI} the NLI variance, with $\mathbb{E}$ its statistical expectation with respect to the random birefringence. A closed formula for such an average variance has been proposed in [19], thus extending the closed-form GN model [13] to include MD, hereafter called the ergodic GN model, and validated in selected cases.

We applied the closed-form ergodic GN model to estimate the impact of MD on the GSNR in selected case studies . Fig. 2(a) shows the GSNR estimated after a single span of length 80 km of an SDM transmission with $N_m = 2$ and 16 strongly-coupled spatial modes carrying complex Gaussian-distributed symbols. In each mode we sent a WDM comb filling the whole C-band with symbol rate 64 Gbaud and spacing 75 GHz. The optical link used an amplifier with noise figure 6.5 dB, a span loss of 17.6 dB, chromatic dispersion 17 ps/nm/km, fiber nonlinear index $n_2 = 2.5 \cdot 10^{-20}$ m^2/W, Manakov correction factor as in [18, eq. (65)]. Since the MIMO is not the focus of this work, at the receiver side we applied an ideal least-square based MIMO, hence with a number of taps equal to the number of symbols, to completely suppress any linear impairment. The ergodic GN model accounted for both self-phase modulation (SPM) and XPM. The plots in Fig. 2 show that for increasing channel power P, the NLI variance grows with P^3 and eventually becomes the dominant impairment, inducing the typical bell shape of the GSNR. The main novelty is that we are able to quantify the improvement brought by MD, which is higher for high mode count N_m, as shown in Fig. 2(a). The GSNR improvement with N_m is monotone, as visible in Fig. 2(b) where we concentrated on the power maximizing the GSNR, i.e., ΔGSNR is the improvement in the maximum GSNR with/without MD. Such improvement in the GSNR has a mild dependence on the chosen symbol rate, as shown in Fig. 2(c) at 48, 64, and 76.8 Gbaud with Nyquist channel spacing. On the contrary, similar relative variations in the SMD coefficient are more relevant, making the impact of MD of larger importance.

The GSNR can be converted into an achievable information rate (AIR). In this work, we evaluate AIR by using the Shannon formula, which, according to mismatched decoding [30], is an achievable limit by a detector optimized for an additive white Gaussian noise channel with the same GSNR. Although the (unknown) capacity of the link is higher, the simple knowledge of the GSNR of the adopted mismatched decoding rule makes the Shannon formula a practical and reliable QoT parameter normally adopted in the literature. For each polarization tributary, the AIR of the discrete equivalent channel model is thus:

$$\text{AIR} = \log_2\left(1 + \text{GSNR}\right) \quad \text{[bits/symbol]}. \tag{3}$$

In this framework, in the next section we evaluate the network capacity accounting for the physical layer impairments by taking into account the gain brought by MD in

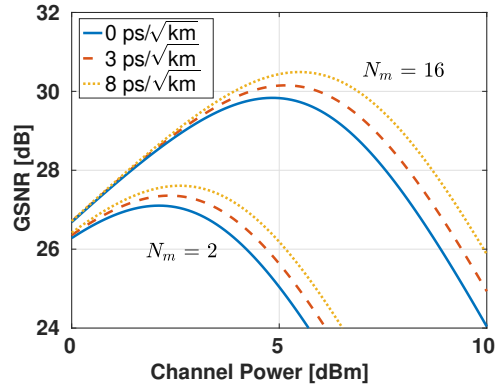

(a)

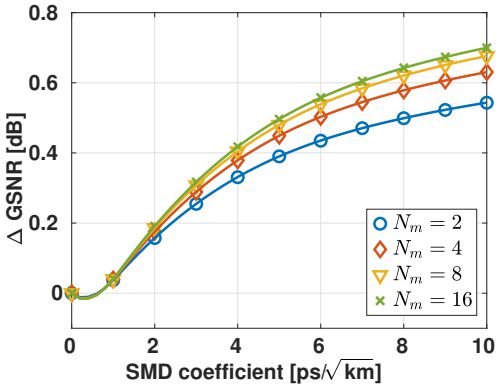

(b)

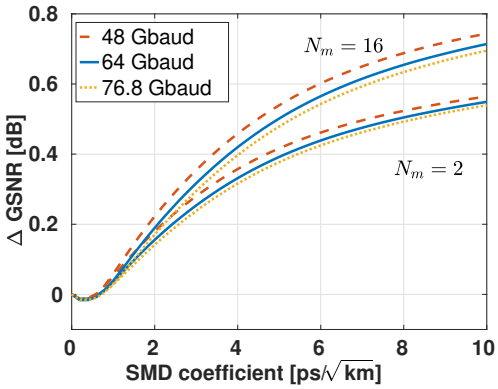

(c)

Figure 2: Full C-band transmission of N_m strongly-coupled spatial modes over a single span. (a) GSNR vs. channel power for different values of the SMD coefficient. (b) Increase of the maximum GSNR value due to mode dispersion for different number of modes. (c) Same as (b), but for variable symbol rates.

mitigating the fiber nonlinearities, usually neglected in the literature because of their high simulation complexity.

III. Network capacity analysis

The network performance is evaluated on two network topologies: the mesh 30-nodes-Spanish backbone shown in [31] with link length values ranging from 80 to 320 km and a ring of 20 nodes with 50-km links. The impact of MD is evaluated at SMD coefficients of 3 and 8 ps/$\sqrt{\text{km}}$. Channel power is optimized according to [32]. First, an analysis of the AIR with complex Gaussian-distributed data is carried out. Then, the AIR constrained to the support of a specific set of modulation formats is evaluated considering a fixed symbol rate. Finally, blocking probability is analyzed assuming fixed connection rate requests.

A. Shannon assumptions: Gaussian-distributed data

The AIR is computed with a GSNR including nonlinear effects in the presence of mode dispersion (3 or 8 ps/$\sqrt{\text{km}}$) and without it. GSNR is computed assuming 64-Gbaud symbol rate and 75-GHz channel spacing. Fig. 3 shows the AIR in bits/symbol averaged on all the possible network paths over the mesh (Fig. 3a) and the ring (Fig. 3b) topologies vs. the number of SDM modes. In particular, the AIR is the achievable information rate per mode and per polarization. We note that the inclusion of MD implies a higher GSNR, thus a higher AIR . The AIR increases with mode dispersion and with the number of modes offered by the fiber spans. In general, the mesh network can achieve a higher capacity since the ring presents a more limited connectivity implying longer routes. As an example, in the mesh topology with 16 modes, AIR is 8.37 bit/symbol (per polarization and mode) without considering mode dispersion, while it is 8.55 bit/symbol with an SMD coefficient of 8 ps/$\sqrt{\text{km}}$. Consequently, in the case of coded channels approaching the channel capacity, for instance with adaptive code rate and probabilistic shaping, MD improves the capacity of a single spatial super-channel by around 368 Gb/s with 16 modes, two polarizations, and 64 Gbaud symbol rate

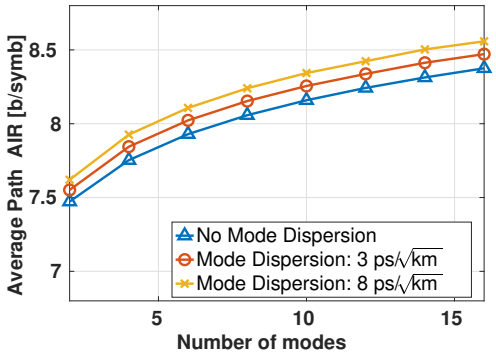

(a)

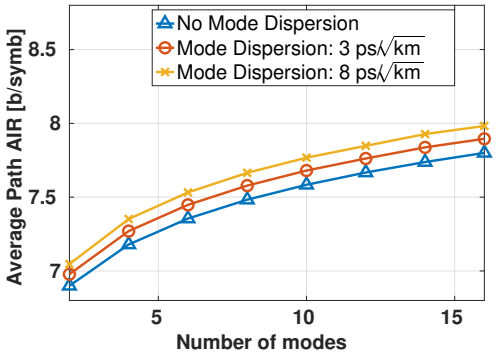

(b)

Figure 3: Average path AIR in: (a) the mesh topology; (b) the ring topology.

Table I: Assumed modulation formats: line rate per mode for 64-Gbaud symbol rate and GSNR threshold (TH').

Modulation format	Supported rate per mode	TH'
PM-64QAM	768 Gb/s	24.6 dB
PM-32QAM	640 Gb/s	21.6 dB
PM-16QAM	512 Gb/s	18.6 dB
PM-8QAM	384 Gb/s	16 dB
PM-QPSK	256 Gb/s	12 dB

B. Achievable network capacity constrained to multiple modulation formats and fixed symbol rate

Evaluations on network capacity are carried out considering fixed symbol rate and a set of possible modulation formats, each one supporting a specific gross rate per mode (assuming 64-Gbaud symbol rate). Each modulation format, to be acceptable, requires a minimum GSNR value, thus requires that GSNR is above a threshold TH'. In this paper, we assume minimum GSNR values TH' as in [33], which are selected to achieve a bit error rate lower than 10^{-3}. Moreover, minimum GSNR values may also include *margins*, typically adopted by network operators to account for effects not considered in the QoT estimation model [16], [17]: e.g., aging, model inaccuracies. Thus, we assume that a given modulation format is supported by a route if the associated GSNR is above the threshold TH, defined as $\text{TH} = \text{TH}' + M$, with M the conservative margins (in dB). Table I summarizes the considered modulation formats with the associated gross rate per mode and the assumed TH' on GSNR. Preference will be given to the selection of higher-order modulation formats, which are more spectral efficient. Connection requests follow a Poisson distribution with mean inter-arrival time $1/\lambda$ and a holding time exponentially distributed with average $1/\mu = 250$s. Network load (λ/μ) is varied through λ. Path computation is performed with load balancing as in [34] and spectrum assignment is first fit. Each connection is switched over a bandwidth of 75 GHz. Depending on the selected path, the most spectral efficient modulation format supported by the computed GSNR over that path (with or without mode dispersion) is chosen, by comparing GSNR against TH values. Then, based on the modulation format, a connection carries a specific rate, as previously mentioned. Table II shows the average overall rate supported by the network considering or not mode dispersion (8 ps/$\sqrt{\text{km}}$), assuming 12 modes in the two network topologies with $M = 1$ dB.

Table II: Average overall network rate [Tb/s] with margin $M=1$ dB in the: (a) mesh topology; (b) ring topology.

(a) Overall rate in the meshed topology

	No Mode Dispersion	8ps/sqrt(km)
100 Erlang	783.9 Tb/s	805.8 Tb/s
150 Erlang	1180.6 Tb/s	1213.5 Tb/s
200 Erlang	1567.9 Tb/s	1611.6 Tb/s
250 Erlang	1959.9 Tb/s	2014.5 Tb/s

(b) Overall rate in the ring topology

	No Mode Dispersion	8ps/sqrt(km)
100 Erlang	702.8 Tb/s	727.1 Tb/s
150 Erlang	1058.5 Tb/s	1095.0 Tb/s
200 Erlang	1404.4 Tb/s	1452.8 Tb/s
250 Erlang	1731.2 Tb/s	1789.2 Tb/s

The overall rate increases with the network load since more connections are active in the network. Mode dispersion permits to increase the overall capacity. Indeed, the higher GSNR values allow using higher-order modulation formats. The improvement can be estimated by modifying the GN model as in [19], at comparable computational effort. As an example, in the ring topology, with 150 Erlang, an increase of 36.5 Tb/s is supported by the network.

C. Blocking probability in the presence of multiple symbol rates and modulation formats

In this subsection, a networking analysis is carried out assuming fixed-rate connection requests. Traffic load is varied as in Sec. III-B. The reference rate is 9.2 Tb/s, achievable with PM-64QAM and 64 GBaud in the presence of 12 spatial modes. In the case of PM-64QAM and assuming a Nyquist bandwidth, the assumed switched bandwidth is 75 GHz. In case a lower-order modulation format is required to be selected when GSNR is below the associated threshold, more carriers or the tuning of symbol rate may be required in order to meet the requested bit rate of 9.2 Tb/s. As an example, with PM-8QAM, such a bit rate is achieved with 64-GBaud symbol rate and 2 carriers, thus requiring more bandwidth than PM-64QAM.

We then studied the blocking probability versus network margin M. Table III shows the assumed transmission parameters required to achieve the target bit rate: modulation format, symbol rate, number of carriers, and spectrum slot width (which, for the ITU-T flex-grid, is a multiple of 12.5 GHz). Note that GSNR depends on the assumed symbol rate.

Table III: Modulation format, symbol rate, number of carriers, and spectrum slot width to achieve 768 Gb/s gross rate per mode, and associated TH'.

Modulation format	Symbol rate	Number of carriers	Spectrum slot width	TH'
PM-64QAM	64 Gbaud	1	75 GHz	24.6 dB
PM-32QAM	76.8 Gbaud	1	87.5 GHz	21.6 dB
PM-16QAM	48 Gbaud	2	112.5 GHz	18.6 dB
PM-8QAM	64 Gbaud	2	137.5 GHz	16 dB
PM-QPSK	64 Gbaud	3	200 GHz	12 dB

Figs. 4, 5, and 6 show the blocking probability versus traffic load in the mesh topology for several values of adopted network margins: $M = 0$ dB, $M = 1$ dB, $M = 2$ dB, respectively. Note that in order to assure a fixed connection rate, we adopted different symbol rate values per modulation format (as in Tab. III), thus the GSNR values which have driven these simulations may be different from the GSNR values of Secs. III-A and III-B. Fig. 4 shows that in the considered scenario, with $M=0$ dB, the network performance in terms of blocking probability are the same considering or not MD. This happens because for all the network paths the GSNR is always within the same range, with and without mode dispersion. As an example, Tab. IV shows the transmission performance of a sample path composed of 5 spans. In all the three cases (without and with mode dispersion), PM-32QAM is selected. Indeed, with $M=0$ dB, the TH associated with PM-32QAM is 21.6 dB and all the reported GSNR values are higher than TH. Unfortunately, to support a higher-order format – PM-64QAM – a GSNR of at least 24.6 dB would be required but in none of the three cases GSNR is enough. Therefore, with and without MD, by fixing a path, with $M=0$ dB in the considered scenario, the same modulation format is always selected.

With $M = 1$ and 2 dB, the threshold TH is shifted and this creates differentiation in the possibilities to select or not a given modulation format. Figs. 5 and 6 show that in the assumed scenario, with 1 or 2 dB of margins, the inclusion of MD in the GN model provides relevant benefits in terms of

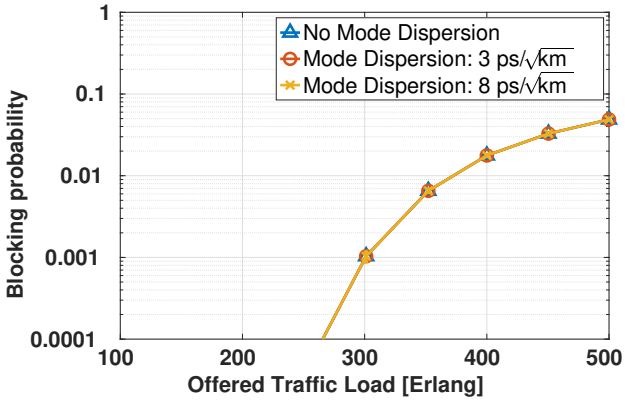

Figure 4: Blocking probability vs. traffic load in the mesh topology with $M=0$ dB.

Table IV: Transmission performance of a sample path of 5 spans with $M = 0$ dB: estimated GSNR and selected modulation format.

No mode dispersion	3 ps/$\sqrt{\text{km}}$	8 ps/$\sqrt{\text{km}}$
22.4 dB, PM-32QAM	22.7 dB, PM-32QAM	22.9 dB, PM-32QAM

blocking probability reduction. As an example, with $M = 1$ dB, the threshold associated with PM-32QAM is TH=22.6 dB. By referring to the GSNR values of the example in Tab. IV, such a threshold is met with 3 and 8 ps/$\sqrt{\text{km}}$, while it is not met without MD. Thus, in the latter case a lower-order modulation format (PM-16QAM) must be selected. Then, a network design based on the ergodic GN model permits to use more frequently higher-order modulation formats, which require less spectrum to support the same fixed line rate: e.g. 87.5 GHz with PM-32QAM instead of 112.5 GHz with PM-16QAM. This implies a lower blocking probability and, thus, a larger capacity. As an example, by referring to Fig. 5, for a blocking of 10^{-2}, the inclusion of mode dispersion permits to support around 330 Erlang instead of 300 Erlang. Mode dispersion of 3 and 8 ps/$\sqrt{\text{km}}$ present similar performance, an indication that with the assumed hard thresholds TH the extra improvement of the 8 ps/$\sqrt{\text{km}}$ case is lost by the granularity of the modulation formats.

Fig. 7 shows that blocking probability increases with M since QoT requirements become more stringent (i.e., larger GSNR thresholds), thus lower-order formats are more frequently used and, consequently, the spectrum is more quickly consumed. The figure confirms that the inclusion of MD provides better networking performance in terms of blocking probability. Note that, as it happens for $M = 0$ dB (see Fig. 4), also the curves at $M = 3$ dB present the same blocking. This depends on the fact that for all the network paths, GSNR values when compared to the specific thresholds (resulting from $M = 3$ dB) always drive the same modulation format selection, with and without modal dispersion.

Similar behaviors are experienced in the ring topology. As an example, Fig. 8 shows the blocking probability versus

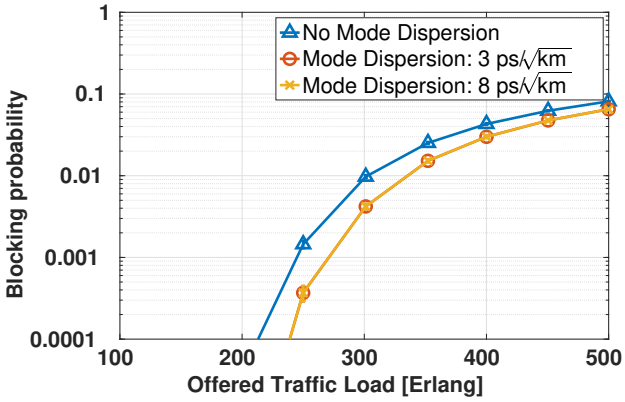

Figure 5: Blocking probability vs. traffic load in the mesh topology with $M = 1$ dB.

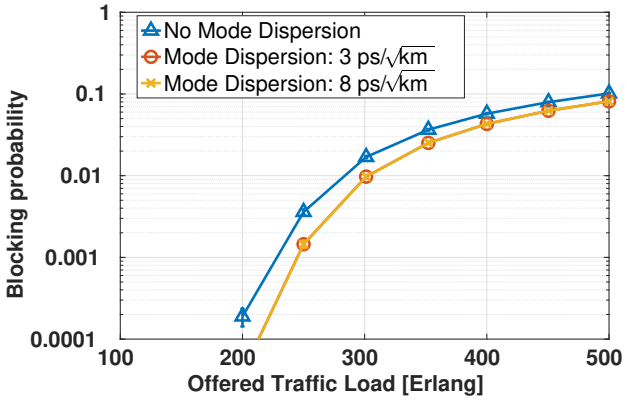

Figure 6: Blocking probability vs. traffic load in the mesh topology with $M = 2$ dB.

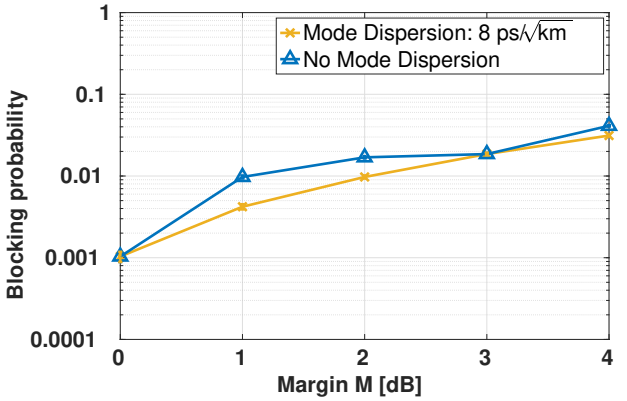

Figure 7: Blocking probability vs. margin M for a network load of 300 Erlang.

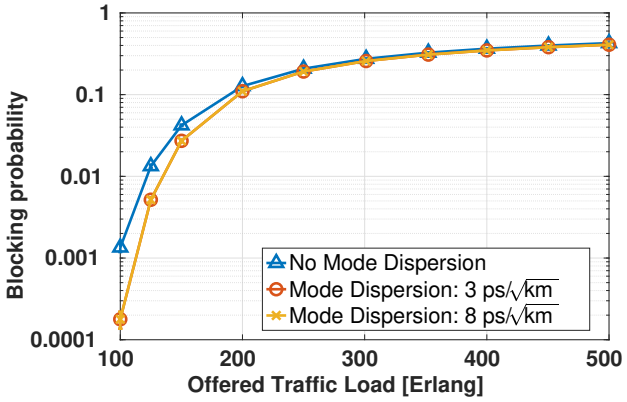

Figure 8: Blocking probability vs. traffic load in the ring topology with $M = 1$ dB.

traffic load when $M = 1$ dB. The presence of MD permits to reduce blocking probability.

IV. Conclusions

We evaluated the impact of mode dispersion on the capacity of upcoming SDM networks exploiting strongly coupled spatial modes. To this purpose, we exploited a GN model extended to account for the interplay between the mode dispersion and the Kerr effect. The AIR with Gaussian-distributed data has been analyzed, showing a capacity increase (that could bring on average to a spatial super-channel capacity increase of almost 400 Gb/s). Then, the network capacity has been investigated considering multiple modulation formats showing an overall network capacity increase (e.g., tens of Tb/s) in the assumed network scenarios. Finally, the analysis of blocking probability has shown that mode dispersion can decrease blocking and, as an example, for a blocking probability of 10^{-2}, accounting for mode dispersion in the QoT estimation may allow increasing the load by 10%.

References

[1] P. J. Winzer, "Scaling optical fiber networks: Challenges and solutions," *Opt. Photon. News*, vol. 26, no. 3, pp. 28–35, Mar 2015.

[2] R. Dar, P. J. Winzer, A. R. Chraplyvy, S. Zsigmond, K.-Y. Huang, H. Fevrier, and S. Grubb, "Cost-optimized submarine cables using massive spatial parallelism," *J. Lightw. Technol.*, vol. 36, no. 18, pp. 3855–3865, 2018.

[3] S. Jain, C. Castro, Y. Jung, J. Hayes, R. Sandoghchi, T. Mizuno, Y. Sasaki, Y. Amma, Y. Miyamoto, M. Bohn, K. Pulverer, M. Nooruzzaman, T. Morioka, S. Alam, and D. J. Richardson, "32-core erbium/ytterbium-doped multicore fiber amplifier for next generation space-division multiplexed transmission system," *Opt. Express*, vol. 25, no. 26, pp. 32 887–32 896, Dec 2017.

[4] N. K. Fontaine, B. Huang, Z. S. Eznaveh, H. Chen, J. Cang, B. Ercan, A. Veláquez-Benitez, S. H. Chang, R. Ryf, A. Schulzgen, J. C. A. Zaharias, P. Sillard, C. Gonnet, J. E. A. Lopez, and R. Amezcua-Correa, "Multi-mode optical fiber amplifier supporting over 10 spatial modes," in *Optical Fiber Communication Conference Postdeadline Papers*. Optica Publishing Group, 2016, p. Th5A.4.

[5] P. M. Krummrich, "Optical amplifiers for multi mode / multi core transmission," in *Optical Fiber Communication Conference*. Optica Publishing Group, 2012, p. OW1D.1.

[6] S. Randel, R. Ryf, A. Sierra, P. J. Winzer, A. H. Gnauck, C. A. Bolle, R.-J. Essiambre, D. W. Peckham, A. McCurdy, and R. Lingle, "6×56-Gb/s mode-division multiplexed transmission over 33-km few-mode fiber enabled by 6×6 MIMO equalization," *Opt. Express*, vol. 19, no. 17, pp. 16 697–16 707, Aug 2011.

[7] R. Ryf, S. Randel, A. H. Gnauck, C. Bolle, A. Sierra, S. Mumtaz, M. Esmaeelpour, E. C. Burrows, R.-J. Essiambre, P. J. Winzer, D. W. Peckham, A. H. McCurdy, and R. Lingle, "Mode-Division Multiplexing Over 96 km of Few-Mode Fiber Using Coherent 6×6 MIMO Processing," *J. Lightw. Technol.*, vol. 30, no. 4, pp. 521–531, 2012.

[8] T. Hayashi, T. Sakamoto, Y. Yamada, R. Ryf, R.-J. Essiambre, N. Fontaine, M. Mazur, H. Chen, and T. Hasegawa, "Randomly-coupled multi-core fiber technology," *Proceedings of the IEEE*, vol. early access, pp. 1–18, 2022.

[9] G. Labroille, P. Jian, N. Barre, B. Denolle, and J.-F. Morizur, "Mode selective 10-mode multiplexer based on multi-plane light conversion," in *2016 Optical Fiber Communications Conference and Exhibition (OFC)*, no. Th3E.5, 2016.

[10] "Cailabs – Proteus-C," https://www.cailabs.com/en/product/proteus-c/.

[11] A. Carena, V. Curri, G. Bosco, P. Poggiolini, and F. Forghieri, "Modeling of the impact of nonlinear propagation effects in uncompensated optical coherent transmission links," *J. Lightw. Technol.*, vol. 30, no. 10, pp. 1524–1539, 2012.

[12] P. Poggiolini, G. Bosco, A. Carena, V. Curri, Y. Jiang, and F. Forghieri, "The GN-model of fiber non-linear propagation and its applications," *J. Lightw. Technol.*, vol. 32, no. 4, pp. 694–721, 2014.

[13] G. Rademacher and K. Petermann, "Nonlinear Gaussian Noise Model for Multimode Fibers with Space-Division Multiplexing," *J. Lightw. Technol*, vol. 34, no. 9, pp. 2280–2287, 2016.

[14] J. M. Gené and P. J. Winzer, "A universal specification for multicore fiber crosstalk," *IEEE Photon. Technol. Lett.*, vol. 31, no. 9, pp. 673–676, 2019.

[15] P. Martelli and P. Boffi, "Crosstalk-Induced Penalty in Coherent Space-Division Multiplexing Transmission," in *2018 20th International Conference on Transparent Optical Networks (ICTON)*, no. We.C1.4, 2018.

[16] Y. Pointurier, "Design of low-margin optical networks," *J. Opt. Commun. Netw.*, vol. 9, no. 1, pp. A9–A17, 2017.

[17] P. Soumplis, K. Christodoulopoulos, M. Quagliotti, A. Pagano, and E. Varvarigos, "Network planning with actual margins," *J. Lightw. Technol.*, vol. 35, no. 23, pp. 5105–5120, 2017.

[18] C. Antonelli, M. Shtaif, and A. Mecozzi, "Modeling of nonlinear propagation in space-division multiplexed fiber-optic transmission," *J. Lightw. Technol.*, vol. 34, no. 1, pp. 36–54, 2016.

[19] P. Serena, C. Lasagni, A. Bononi, C. Antonelli, and A. Mecozzi, "The Ergodic GN Model for Space-Division Multiplexing with Strong Mode Coupling," *J. Lightw. Technol.*, vol. 40, no. 10, pp. 3263–3276, May 2022.

[20] H. Tode and Y. Hirota, "Routing, spectrum, and core and/or mode assignment on space-division multiplexing optical networks [invited]," *J. Opt. Commun. Netw*, vol. 9, no. 1, pp. A99–A113, 2017.

[21] C. Rottondi, P. Boffi, P. Martelli, and M. Tornatore, "Routing, modulation format, baud rate and spectrum allocation in optical metro rings with flexible grid and few-mode transmission," *J. Lightw. Technol.*, vol. 35, no. 1, pp. 61–70, 2017.

[22] M. Yaghubi-Namaad, A. G. Rahbar, and B. Alizadeh, "Adaptive modulation and flexible resource allocation in space-division-multiplexed elastic optical networks," *J. Opt. Commun. Netw*, vol. 10, no. 3, pp. 240–251, 2018.

[23] M. Yang, Y. Zhang, and Q. Wu, "Routing, spectrum, and core assignment in SDM-EONS with MCF: node-arc ILP/MILP methods and an efficient XT-aware heuristic algorithm," *J. Opt. Commun. Netw*, vol. 10, no. 3, pp. 195–208, 2018.

[24] G. Savva, G. Ellinas, B. Shariati, and I. Tomkos, "Physical layer-aware routing, spectrum, and core allocation in spectrally-spatially flexible optical networks with multicore fibers," in *2018 IEEE International Conference on Communications (ICC)*, 2018, pp. 1–6.

[25] C. Rottondi, P. Martelli, P. Boffi, L. Barletta, and M. Tornatore, "Crosstalk-aware core and spectrum assignment in a multicore optical link with flexible grid," *IEEE Trans. Commun.*, vol. 67, no. 3, pp. 2144–2156, 2019.

[26] Z. Luo, S. Yin, L. Zhao, Z. Wang, W. Zhang, L. Jiang, and S. Huang, "Survivable routing, spectrum, core and band assignment in multi-band space division multiplexing-elastic optical networks," *J. Lightw. Technol.*, vol. 40, no. 11, pp. 3442–3455, March 2022.

[27] P. Boffi, N. Sambo, P. Martelli, P. Parolari, A. Gatto, F. Cugini, and P. Castoldi, "Mode-group division multiplexing: Transmission, node architecture, and provisioning," *J. Lightw. Technol.*, vol. 40, no. 8, pp. 2378–2389, 2022.

[28] N. Sambo, C. Lasagni, P. Serena, P. Castoldi, and A. Bononi, "Impact of modal dispersion on the performance of an SDM optical network," in *Proc. of ONDM*, 2022.

[29] T. Hayashi *et al.*, "Field-deployed multi-core fiber testbed," in *Proc. of OECC and PSC*, no. PDP3, 2019.

[30] D. Arnold, H. Loeliger, P. Vontobel, A. Kavcic, and W. Zeng, "Simulation-Based Computation of Information Rates for Channels With Memory," *IEEE Trans. Inf. Theory*, vol. 52, no. 8, pp. 3498–3508, Aug. 2006.

[31] N. Sambo, B. Correia, A. Napoli, J. Pedro, L. Kiani, P. Castoldi, and V. Curri, "Network upgrade exploiting multi band: S- or E-band?" *Journal of Optical Communications and Networking*, vol. 14, no. 9, pp. 749–756, 2022.

[32] P. Poggiolini, G. Bosco, A. Carena, V. Curri, Y. Jiang, and F. Forghieri, "The GN-model of fiber non-linear propagation and its applications," *J. Lightw. Technol.*, vol. 32, no. 4, pp. 694–721, 2013.

[33] A. Mitra, D. Semrau, N. Gahlawat, A. Srivastava, P. Bayvel, and A. Lord, "Effect of Channel Launch Power on Fill Margin in C+L Band Elastic Optical Networks," *J. Lightw. Technol.*, vol. 38, no. 5, pp. 1032–1040, 2020.

[34] N. Sambo, F. Cugini, G. Bottari, G. Bruno, P. Iovanna, and P. Castoldi, "Lightpath provisioning in wavelength switched optical networks with flexible grid," in *2011 European Conference on Optical Communication (ECOC)*, no. We.10.P1.96, 2011.